Tensile and Flammability Properties of Polypropylene-based RTPO/Clay Nanocomposites for Cable Insulating Material

Chae Hwan Hong,[1] Yong Bum Lee,[1] Jin Woo Bae,[1] Jae Young Jho,[1] Byeong Uk Nam,[2] Gi Joon Nam,[3] Kun Joo Lee[3]

[1]*Hyperstructured Organic Materials Research Center and School of Chemical and Biological Engineering, Seoul National University, Seoul 151–742, Korea*
[2]*Department of Applied Chemical Engineering, Korea University of Technology and Education, Chungnam 330–708, Korea*
[3]*Polymer Technology Group, Research & Development Center, LG Cable Ltd., 555 Kyungki 431–080, Korea*

Received 18 January 2005; accepted 7 February 2005
DOI 10.1002/app.21842
Published online in Wiley InterScience (www.interscience.wiley.com).

ABSTRACT: Nanocomposites of polypropylene-based RTPO with organically modified clays were prepared by melt compounding of three components, that is, polypropylene-based RTPO, maleic anhydride-grafted polypropylene oligomer (PP*g*MA), and organically modified clay. Their morphologies, tensile behaviors, and flammability properties were investigated. In the clay nanocomposites, the silicate layers were dispersed at the nanometer level, which was confirmed by X-ray diffraction and transmission electron microscopy. The tensile yield strength of nanocomposites containing 10 wt % clay exhibited 2.8 times higher value compared with that of neat resin. The combustion behavior of the nanocomposites was evaluated by measuring the heat release rate (HRR) using cone calorimetry. The peak HRR was lowered greatly and the char yield was very high compared with those of neat resin. However, these flame retardant properties of clay are not sufficient as a flame retardant used alone in cable applications. © 2005 Wiley Periodicals, Inc. J Appl Polym Sci 97: 2375–2381, 2005

Key words: clay; flame retardance; mechanical properties; nanocomposite; polypropylene

INTRODUCTION

Nanocomposites based on organic polymers and inorganic clay materials consisting of silicate layers such as montmorillonite (MMT) have attracted a great deal of interest because they frequently exhibit unexpected hybrid properties synergistically derived from the two components, including superior mechanical properties, reduced gas permeability, improved solvent resistance, and enhanced flame retardant properties. A large number of polymer/clay nanocomposites have been studied, including polystyrene,[1] polyamide,[2] polyimide,[3] epoxy resin,[4] and polypropylene.[5–20] Polypropylene (PP)/clay nanocomposites by direct melt compounding of PP with organic MMT in the presence of maleic anhydride-grafted PP (PP*g*MA) were first developed by researchers at Toyota.[6] They added three times as much PP*g*MA as the clay by weight in preparing well-mixed PP/clay nanocomposites. Thereafter, the melt compounding method has become mainstream in the preparation of PP/clay nanocomposites, although the result of an *in situ* polymerization method was reported recently.[9] One of the interesting properties of nanocomposites is their flame retardant properties, namely, a significant decrease in the peak heat release rate (HRR) and a change in the char structure. These properties of clay are expected as a new synergistic flame retardant system that will work with conventional inorganic flame retardants.[21–23]

Recently, there has been a great demand to develop PP based resin as an insulating material for cable applications in the cable industry. This is particularly true for automotive cable insulation applications where plasticized PVC and PE/EVA are the main polymers currently used. PVC, although a better fire retardant polymer than polyolefins, is a source of health and environmental problems due to potentials for release of chlorine-containing chemicals. PE/EVA, on the other hand, has a certain limitation in its low application temperature. Therefore, it is expected that PP is the most promising material to replace PVC or PE/EVA. For the application of PP type resin for cable insulating materials, not only flame retardancy but also flexibility and tensile properties, for example, tensile strength and elongation at break, must be satisfied. Although the advantages of PP are good resistance to high temperature, low thermal expansion, and excellent dielectric properties, the main drawbacks of PP are embrittlement at low temperature and

Correspondence to: J. Y. Jho (jyjho@snu.ac.kr).

TABLE I
Compounding Formulations and Tensile Properties of PP-Based RTPO/PPgMA/Clay Nanocomposites

Sample code	PP-Based RTPO [wt %]	PPgMA [wt %]	Clay [wt %]	Tensile strength @ yield [MPa]	Tensile strength @ break [MPa]	Elongation @ break [%]	Tensile modulus [MPa]
RTPO (neat)	100	0	0	5.1	20.6	1390	46.0
RTPO NC3	88	9	3	6.4	16.6	980	71.2
RTPO NC5	80	15	5	8.1	16.8	859	78.3
RTPO NC10	60	30	10	14.2	16.6	437	251

rigidity. Moreover, Hasegawa and coworkers reported that the elongation at break of PP/clay nanocomposites worsens more than that of neat resin.[7] Therefore, for the application of PP type resin as a cable insulating material and for the use of clay as a new flame retardant, it is important to choose a suitable PP matrix resin that has a controlled balance between flexibility and rigidity.

Generally, the flexibility of PP can be improved by blending with poly(ethylene-*co*-propylene) (EPR). The PP/EPR blends are called toughened PP, which finds wide applications in the consumer industry. Besides PP/EPR blends prepared by mechanical blending, blends prepared by *in situ* or in-reactor blending techniques have been developed. This technique involves the bulk polymerization of propylene, followed by the gas-phase copolymerization of ethylene and propylene driven by the spherical superactive $TiCl_4$/$MgCl_2$ based catalyst system. This material is called PP-based RTPO or in-reactor made TPO.[24–26] This technique allows the production of innovative polyolefin materials and multiphase blends directly in the reactor. It has made possible a wide range of new products, including soft, flexible PP produced without rubber blending mechanically. Because the rubber phase can be dispersed uniformly and reach a high degree of dispersion in these *in situ* blends, it is possible to make more intimate interaction between the matrix and the rubber phase. Therefore, RTPO is expected to be the most suitable matrix resin for PP type cable insulating materials.

The objective of this study is to prepare PP-based RTPO/clay nanocomposites by using PP*g*MA as a compatibilizer and to investigate their tensile properties and flame retardant properties for the application of cable insulating material.

EXPERIMENTAL

Materials

Polypropylene-based RTPO used in this study was Adflex, Q100F, which is a soft thermoplastic polypropylene plastomer made by Basell's Catalloy process (Density = 0.890 g/cm^3, Melt Flow Rate = 0.6 g/10 min at 230°C, 2.16 kg load). Random PP used in this study was R724J supplied by LG-Caltex Company, Korea (Density = 0.90 g/cm^3, Melt Flow Rate = 1.9 g/10 min at 230°C, 2.16 kg load). Ethylene-propylene rubber used in this study was KEP-020P supplied by Kumho PolyChem, Korea (ethylene content 71 wt %, Melt Flow Rate = 3.2 g/10 min at 230°C, 2.16 kg load). Maleic anhydride grafted-polypropylene (PP*g*MA) containing 2.6 wt % maleic anhydride was supplied by Honam Petrochemical Company, Korea (M_w = 49,600, M_w/M_n = 2.2). The commercial organic modified MMT, Cloisite® 20A, supplied by Southern Clay Products was used, which was ion-exchanged with dimethyl di(hydrogenated tallow) ammonium ions. (Tallow was composed predominantly of dodecyl chains with a smaller amount of lower homologues. The approximate composition was C18 65%, C16 30%, and C14 5%.) Magnesium hydroxide (MDH), employed as flame retardant, was a high purity untreated grade (Magnifin H5) supplied by Martinswerk GmbH. The average particle size was 1.0 μm, and the specific surface area was 5.0 m^2/g.

Compounding

For the composite formation, PP*g*MA, organically modified clay, and MDH were dry mixed with PP-based RTPO and melt compounded in a mixing head (Haake Rheomix 600, Haake Rheocord 9000 system). Their compounding formulations are listed in Tables I,

TABLE II
Compounding Formulations and Tensile Properties of PP/EPR/PPgMA/Clay Composites

Sample code	Random-PP [wt %]	EPR [wt %]	PPgMA [wt %]	Clay [wt %]	Tensile strength @ yield [MPa]	Tensile strength @ break [MPa]	Elongation @ break [%]
PPEPR-1	30	30	30	10	-	8.7	40
PPEPR-2	40	20	30	10	-	9.8	51

TABLE III
Compounding Formulations and Tensile Properties of PP-Based RTPO/PPgMA/Clay/MDH Composites

Sample code	PP-based RTPO [wt %]	PPgMA [wt %]	Clay [wt %]	MDH [wt %]	Tensile strength @ yield[MPa]	Tensile strength @ break [MPa]	Elongation @ break [%]
PP-1	36	0	4	60	8.5	9.4	210
PP-2	34	2	4	60	8.7	10.2	168
PP-3	32	4	4	60	8.7	10.3	138
PP-4	30	6	4	60	9.3	11.7	82
PP-5	28	8	4	60	10.4	14.2	71

II, and III. The weight ratio of clay to PP*g*MA was 1/3. Each sample was prepared at 180°C with the rotor speed 100 rpm for 10 min. Upon completion of compounding, the molten polymer was removed and then compression molded at 190°C and 15 metric tons of pressure to prepare a test specimen.

Characterization

X-ray diffraction (XRD) was carried out by using a Rigaku X-ray generator (Cu Kα radiation with λ = 0.15,406 nm, generator voltage = 30 kV, current = 45 mA) at room temperature. The diffractograms were scanned in 2θ ranges from 1.5 to 10° at a rate of 1°/min. Measurements were recorded at every 0.03°. For comparative purposes, the XRD patterns were represented in terms of relative intensities; the intensity of the strongest reflection was arbitrarily assigned a value of d_{001}, the interplanar distance of layered clay.

Bright field transmission electron microscopy (TEM) images of PP-based RTPO/clay composites and the corresponding combustion chars were obtained at 120 kV operating power with a Phillips CM 20. The composite samples, embedded in an epoxy resin and cured at 80°C overnight, were microtomed to give sections with a thickness of 70 nm. Combustion chars were broken into small pieces, embedded in an epoxy resin, and microtomed in a similar way. Ultrathin sections were prepared with a 45° diamond knife using a Leica Ultracut UCT microtome. The sections were transferred from water to carbon-coated Cu grids of 200 mesh. The contrast between the layered silicates and the polymer or char phase was sufficient for imaging, so no heavy metal staining of sections prior to imaging was required.

Rheological measurements were carried out in an oscillatory mode on a rheometer (Rheometrics RMS-800) equipped with a parallel plate geometry using 25 mm diameter plates at 180°C in a nitrogen environment. The samples were subjected to oscillatory shear over a frequency range of 0.01–100 rad/s. A strain amplitude of 2% was applied during the measurement, and the data were recorded only when the torque amplitude was above the recommended threshold of 2 g cm. The measurements were recorded within 30 min of loading the sample on the platen and were reproducible.

The tensile strength and elongation at break were determined using a universal testing machine at 25°C according to ASTM D 638, and the head speed was 50 mm/min. Samples were prepared from 1.0 mm thick compression molding sheets, from which test specimens were cut using a die. All measurements were done in five replicates and the values averaged.

Evaluations of flammability were achieved using a Fire Testing Technology cone calorimeter from LG Cable Ltd., according to ASTM E 1354–92. The testing sample was a 100 × 100 × 3 mm^3 thick specimen prepared by compression molding at 190°C and 15 metric tons of pressure. The tests were performed at an incident heat flux of 35 kW/m^2. Peak heat release rate, mass loss rate, specific extinction area, carbon monoxide, and heat of combustion data were collected. The cone data reported here are the average of two or three replicated experiments. Limiting Oxygen Index (LOI) was measured in a Stanton-Redcroft LOI according to ASTM 2863–98.

RESULTS AND DISCUSSION

Structural analysis of nanocomposites

The dispersibilities of the clay layers in the matrix resin were evaluated using XRD and TEM. Figure 1

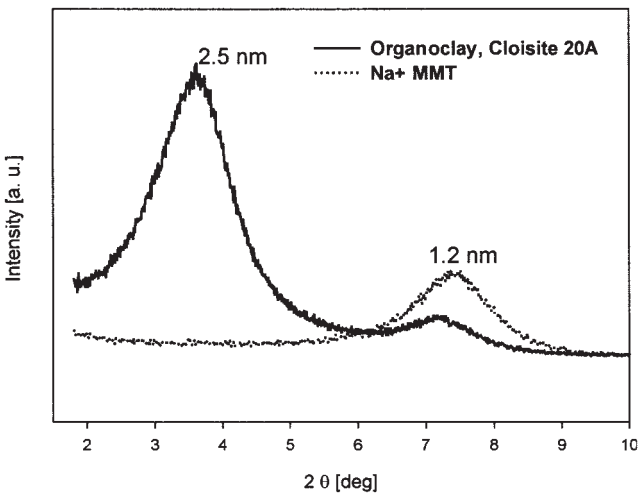

Figure 1 X-ray diffraction patterns of Na^+ MMT and organic modified MMT, Cloisite® 20A.

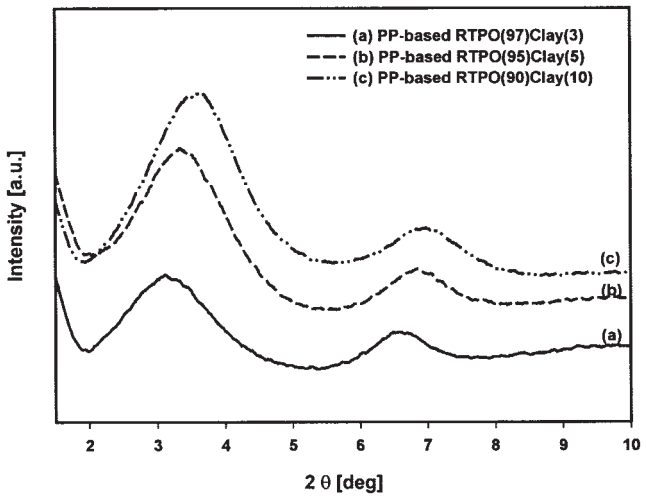

Figure 2 X-ray diffraction patterns of the PP-based RTPO/clay without PP*g*MA: (a) PP-based RTPO (97 wt %)/clay (3 wt %), (b) PP-based RTPO (95 wt %)/clay (5 wt %), (c) PP-based RTPO (90 wt %)/clay (10 wt %).

shows the XRD patterns of Na^+ MMT and organic modified MMT, Cloisite® 20A. The latter exhibited two well-defined peaks. The characteristic diffraction peak d_{001} is located at around 3.4°, corresponding to a basal interlayer spacing of 2.5 nm according to Bragg's equation. Figure 2 shows the XRD patterns of the PP-based RTPO/clay composites prepared without PP*g*MA. The reflection peaks arising from the clay were observed at $2\theta = 3.3 \sim 3.6°$, which indicates that the silicate layers still keep an ordered multi-layer structure. However, there were no peaks in the XRD patterns of the PP-based RTPO/PP*g*MA/clay nanocomposites in Figure 3. This indicates that PP chains alone could not intercalate between the layers, and the

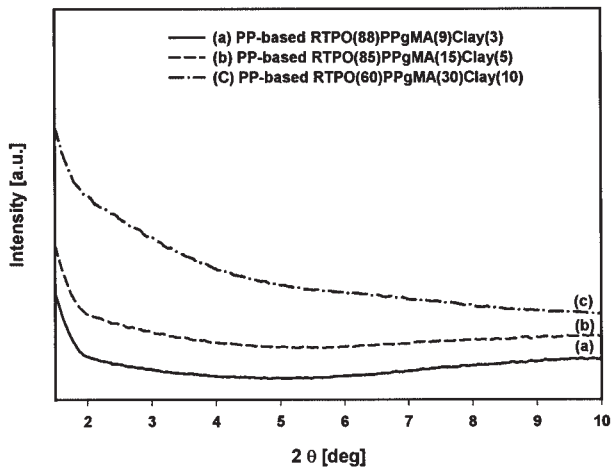

Figure 3 X-ray diffraction patterns of the PP-based RTPO/clay with PP*g*MA: (a) PP-based RTPO (88 wt %)/PP*g*MA (9 wt %)/clay (3 wt %), (b) PP-based RTPO (85 wt %)/ PP*g*MA (10 wt %)/clay (5 wt %), (c) PP-based RTPO (60 wt %)/ PP*g*MA (30 wt %)/clay (10 wt %).

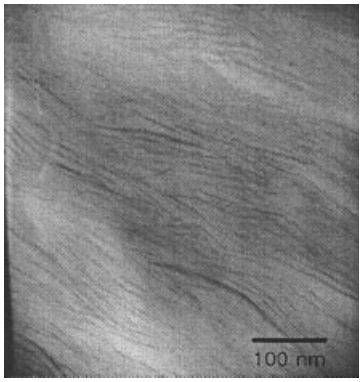

Figure 4 TEM image of PP-based RTPO/PP*g*MA/clay nanocomposite containing 10 wt % clay, 30 wt % PP*g*MA.

chains of the PP*g*MA could be intercalated into the clay interlayers through hydrogen bonding between the polar functional group of PP*g*MA and the oxygen group of the silicates. To further confirm the dispersion state of the clay in the matrix in more detail, a TEM experiment was carried out. Figure 4 presents the TEM image of sample RTPO NC 10 at a magnification of 150,000. The dark lines represent the silicate layers, and individual silicate layers of about 1 nm thickness can be seen. Thus, the TEM image is in agreement with X-ray measurements.[27]

The storage modulus (G′) data resulting from the dynamic frequency sweep measurements for PP-based RTPO/PP*g*MA/clay nanocomposites with varying clay contents are compared. Figure 5 shows the effect of the clay content on G′ of the nanocomposites, in which the magnitude of G′ increased with clay content at low frequency. It is believed that the degree of dependence of G′ on the low frequency reflects sensitively the effect of clay on the viscoelastic

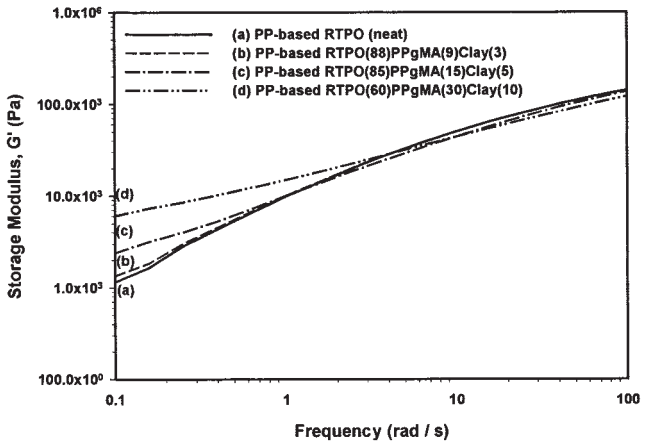

Figure 5 Storage modulus curves of neat resin and three PP-based RTPO/clay with PP*g*MA: (a) PP-based RTPO (neat), (b) PP-based RTPO (88 wt %)/PP*g*MA (9 wt %)/clay (3 wt %), (c) PP-based RTPO (85 wt %)/PP*g*MA (10 wt %)/clay (5 wt %), (d) PP-based RTPO (60 wt %)/PP*g*MA (30 wt %)/clay (10 wt %).

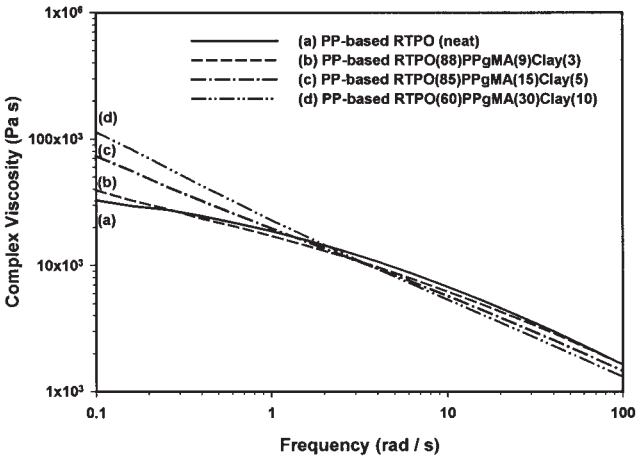

Figure 6 Viscosity curves of neat resin and three PP-based RTPO/clay with PP*g*MA: (a) PP-based RTPO (neat), (b) PP-based RTPO (88 wt %)/PP*g*MA (9 wt %)/clay (3 wt %), (c) PP-based RTPO (85 wt %)/PP*g*MA (10 wt %)/clay (5 wt %), (d) PP-based RTPO (60 wt %)/PP*g*MA (30 wt %)/clay (10 wt %).

properties of the nanocomposites. From comparison of the terminal slope of G′ versus frequency, the G′ behavior of sample RTPO NC 3 is quite similar to that of the neat PP-based RTPO matrix. With clay content 5 wt %, the dependence of G′ on frequency decreases in the terminal zone, and the G′ curve of sample RTPO NC 10 exhibits a plateau at low frequency. This indicates that the viscoelastic properties are still dominated by the matrix resin when the clay content is below 3 wt %, and PP-based RTPO nanocomposites may experience a transition from liquid-like behavior to solid-like behavior with the clay content 5 wt %. The reason for this at low frequency is the increase of interfacial energy due to the finely exfoliated nanoparticles. Figure 6 shows the increase of the viscosity of PP-based RTPO nanocomposites with an increase of the clay loading. As the clay content increases, the viscosity level also increases at low frequency and the slope increases sharply from the clay content 5 wt %. According to the LOI testing results in Table IV, no melt drop occurred with the clay content 5 and 10 wt %. Therefore, it would be expected that the increase of viscosity may be a positive effect in relation to the burning behavior.

Mechanical properties

Table I shows the results of the tensile test of the clay nanocomposites. The tensile moduli of the nanocomposites become higher as the content of clay increases. The modulus of nanocomposites containing 10 wt % clay is 5.4 times higher than that of neat resin. The elongation at break decreases as the content of clay increases, but the value of nanocomposites containing 10 wt % clay is 437%, which is much higher than that of PP/clay nanocomposites reported elsewhere.[7] To the author's knowledge, these elongational properties of PP-based RTPO/clay nanocomposites are unique and promising to the application of cable insulating materials.

For comparison with the tensile properties of PP/EPR mechanical blend matrix composites, PP/EPR/PP*g*MA/clay composites were prepared by the same preparation method. Table IV shows the compounding formulation and tensile properties of PP/EPR clay composites. The elongation at break values were about 50%, which was much lower than those of RTPO clay nanocomposites and is not suitable for industrial application. This difference is assumed to be because of the difference of dispersion homogeneity and domain size of ethylene copolymer between RTPO and PP/EPR mechanical blends. Ongoing research is aimed at the effect of domain size and dispersion morphology of EPR domains on the tensile properties of nanocomposites.

Flammability

Heat release rate (HRR) plots of PP-based RTPO neat resin, microcomposites, and nanocomposites are shown in Figure 7. Cone Calorimetry is one of the most effective bench-scale methods for studying the flammability properties of materials. The HRR, in particular the peak HRR, has been found to be the most important parameter to evaluate fire safety.[28] The peak HRR of the nanocomposite containing 10 wt % clay is 37% lower than that of neat resin. On the other hand, the microcomposite shows very similar behavior to the neat resin. At the end of combustion, the neat resin leaves no residue and the microcomposite leaves only a little powder, while the nanocomposite leaves a consistent char-like residue.[21,22]

TABLE IV
Results of Limiting Oxygen Index (LOI) Test of PP-based RTPO/PPgMA/Clay Nanocomposites

Sample code	PP-based RTPO [wt %]	PPgMA [wt %]	Clay [wt %]	LOI index	Remarks
RTPO (neat)	100	0	0	18	melt flow from the top
RTPO NC3	88	9	3	18	melt flow from the top
RTPO NC5	80	15	5	18.5	no melt flow from the top
RTPO NC10	60	30	10	19	no melt flow from the top, compact residue

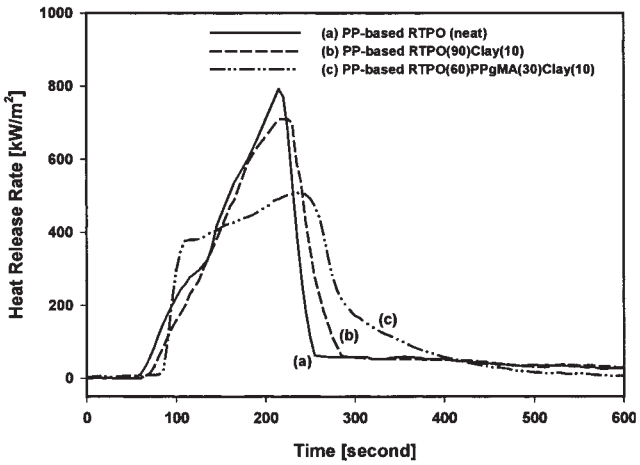

Figure 7 Heat release rate measured with a cone calorimeter (heat flux 35 kW/m^2) for various PP-based RTPO materials: (a) PP-based RTPO (neat resin), (b) PP-based RTPO/clay microcomposite, containing 10 wt % clay, (c) PP-based RTPO/PP*g*MA/clay nanocomposite, containing 10 wt % clay, 30 wt % PP*g*MA.

Figure 8 shows the combustion residue of RTPO NC 10. Comparison of the residues reveals a dramatic improvement in the char formation in clay nanocomposites, and the structure of char appears to be forced to keep the original specimen shape. Generally, PP thermally degrades to volatile products above 250°C through a radical chain process propagated by carbon centered radicals originated by carbon–carbon bond scission. In neat resin, this thermal degradation continues during the combustion, and all intermediate degradation products volatilize completely. On the other hand, there may be physical-chemical adsorption of the intermediate degradation products on the clay surface in clay nanocomposites. This adsorption between the polymer chains and the clay surface may delay fast volatilization of the degradation products and accumulate the incomplete degradation products on the clay surface.

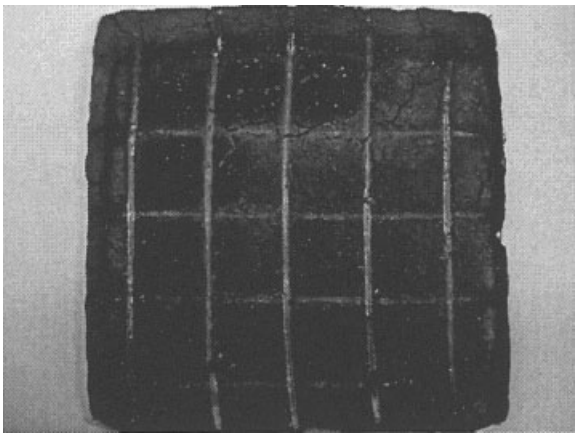

Figure 8 Combustion residue image of PP-based RTPO/PP*g*MA/clay nanocomposite containing 10 wt % clay.

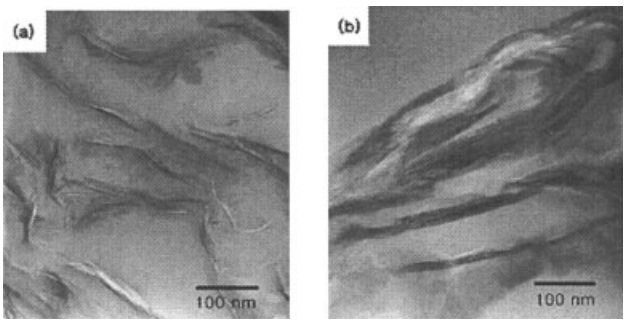

Figure 9 TEM images of combustion residue of (a) PP-based RTPO/PP*g*MA/clay nanocomposite, containing 10 wt % clay, 30 wt % PP*g*MA, (b) PP-based RTPO/clay microcomposite, containing 10 wt % clay.

TEM images of a section of the combustion chars from the nanocomposite and microcomposite are shown in Figure 9. Several multilayered clay structures are seen in the TEM image of the nanocomposite. These multilayered structures might be formed from the collapse of fairly dispersed clay layers during combustion.[21,29,30] But the aggregated structures of clays, which might be formed in the previous compounding step, are seen in the TEM image of the microcomposite. From these results, one possible mechanism to explain how the peak HRR of the clay nanocomposite is lower than that of neat resin, is the formation of a carbonaceous residue with high thermal stability that acts as a protective barrier by reducing the heat and mass transfer between the flame and the polymer and the progressive increase of the barrier effect induced by reassembly of the clay layers.[21,22] But these flame retardant properties of clay are not sufficient as a flame retardant used alone in cable applications because the HRR of the clay nanocomposite is high and LOI is low, which cannot be applicable for industrial cable applications. Therefore, it is expected that clay can be used only as a additive flame retardant with a conventional flame retardant, such as magnesium hydroxide.[31,32]

We prepared RTPO/PP*g*MA/clay/MDH composites containing 60 wt % MDH. Table III shows the compounding formulation and tensile properties. For the clay exfoliation and the control of tensile properties, PP*g*MA content was varied. The tensile strength

TABLE V
Results of Limiting Oxygen Index (LOI) Test of PP-based RTPO/MDH and PP-Based RTPO/Clay/PPgMA/MDH Composites

Sample code	PP-Based RTPO [wt %]	PPgMA [wt %]	Clay [wt %]	MDH [wt %]	LOI index
PPMDH-1	40	0	0	60	25.5
PPMDH-2	34	2	4	60	27

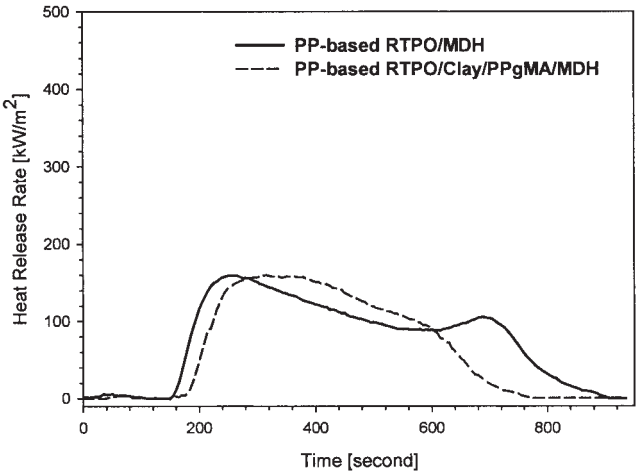

Figure 10 Heat release rate measured with a cone calorimeter (heat flux 35 kW/m^2) of PP-based RTPO/MDH and PP-based RTPO/clay/PP*g*MA/MDH composites.

and elongation at break of sample PP-2 is applicable for practical cable insulating materials. Table V shows the LOI results of PP-based RTPO/MDH and PP-based RTPO/clay/PP*g*MA/MDH composites, respectively. Figure 10 shows the HRR measured with a cone calorimeter (heat flux 35 kW/m^2) of PP-based RTPO/MDH and PP-based RTPO/clay/PP*g*MA/MDH composites. The latter shows the higher LOI and somewhat lower and different HRR values compared with those of the simple PP-based RTPO/MDH composite. Ongoing research is aimed at the surface treatment of MDH and the addition of an interfacial agent on the tensile properties of resin/MDH composites.

CONCLUSIONS

In this work, PP-based RTPO/clay nanocomposites have been prepared by melt compounding by adding the compatibilizer PP*g*MA. The tensile yield strength increased with an increase in the clay content compared to the neat resin, and the elongation at break decreased. However, the values of tensile yield strength and elongation at break of 10 wt % clay nanocomposite reveal that PP-based RTPO/PP*g*MA/clay nanocomposite can be applicable for cable applications. These tensile properties are attributed to the unique morphological characteristics of PP-based RTPO, which has a well dispersed EPR phase in the PP matrix and intimate contact between them. The combustion in cone calorimetry indicated that the peak HRR of clay nanocomposites was much lower than that of neat resin. The char yield was very high, and the char structure was rigid and showed only small cracks. Significant improvements in flame retardancy provided by the layered clay offer the possibility of decreasing the level of a conventional inorganic flame retardant such as magnesium hydroxide, and combinations of layered clay with conventional flame retardants are expected as new flame retardant systems.

The authors gratefully acknowledge the financial support of LG Cable Ltd., South Korea.

References

1. Vaia, R. A.; Jandt, K. D.; Kramer, E. J.; Giannelis, E. P. Chem Mater 1996, 8, 2628.
2. Wu, Z. G.; Zhou, C. X.; Qi, R. R.; Zhang, H. B. J Appl Polym Sci 2002, 83, 2403.
3. Tyan, H. L.; Liu, Y. C.; Wei, K. H. Polymer 1999, 40, 4877.
4. Frohlich, J.; Thomann, R.; Mulhaupt, R. Macromolecules 2003, 36, 7205.
5. Usuki, A.; Kato, M.; Okada, A.; Kurauchi, T. J Appl Polym Sci 1997, 63, 137.
6. Kawasumi, M.; Hasegawa, N.; Kato, M.; Usuki, A.; Okada, A. Macromolecules 1997, 30, 6333.
7. Hasegawa, N.; Kawasumi, M.; Kato, M.; Usuki, A.; Okad, A. J Appl Polym Sci 1998, 67, 87.
8. Marchant, D.; Jayaraman, K. Ind Eng Chem Res 2002, 41, 6402.
9. Sun, T.; Garces, J. M. Adv Mater 2002, 14, 128.
10. Galgali, G.; Ramesh, C.; Lele, A. Macromolecules 2001, 34, 852.
11. Reichert, P.; Hoffmann, B.; Bock, T.; Thomann, R.; Mulhaupt, R.; Friedrich, C. Macromol Rapid Commun 2001, 22, 519.
12. Ellis, T. S.; Angelo, J. S. J Appl Polym Sci 2003, 90, 1639.
13. Gu, S.; Ren, J.; Wang, Q. J Appl Polym Sci 2004, 91, 2427.
14. Wang, Y.; Chen, F.; Wu, K. J Appl Polym Sci 2004, 93, 100.
15. Li, J.; Zhou, C.; Gang, W. Polym Test 2003, 22, 217.
16. Li, J.; Zhou, C.; Wang, G.; Zhao, D. J Appl Polym Sci 2003, 89, 3609.
17. Hasegawa, N.; Okamoto, H.; Kato, M.; Usuki, A. J Appl Polym Sci 1918 2000, 78.
18. Tang, Y.; Hu, Y.; Wang, S.; Gui, Z.; Chen, Z.; Fan, W. J Appl Polym Sci 2003, 89, 2586.
19. Liu, X.; Wu, Q. Polymer 2001, 42, 10013.
20. Hasegawa, N.; Usuki, A. J Appl Polym Sci 2004, 93, 464.
21. Gilman, J. W.; Jackson, C. L.; Morgan, A. B.; Harris, R.; Manias, E.; Giannelis, E. P.; Wuthenow, M.; Hilton, D.; Phillips, S. H. Chem Mater 2000, 12, 1866.
22. Gilman, J. W. App Clay Science 1999, 15, 31.
23. Beyer, G. Fire Mater 2001, 25, 193.
24. Galli, P.; Vecellio, G. Prog Polym Sci 2001, 26, 1287.
25. Galli, P.; Haylock, J. C. Makromol Chem Macromol Symp 1992, 63, 19.
26. Cecchin, G. Macromol Symp 1994, 78, 213.
27. Morgan, A. B.; Gilman, J. W. J Appl Polym Sci 2003, 87, 1329.
28. Babrauskas, V.; Peacock, R. D. Fire Safety J 1992, 18, 255.
29. Du, J.; Wang, D.; Wilkie, C. A.; Wang, J. Polym Degrad Stab 2003, 79, 319.
30. Kashiwagi, T.; Harris, R. H.; Zhang, X.; Briber, R. M.; Cipriano, B. H.; Raghavan, S. R.; Awad, W. H.; Shields, J. R. Polymer 2004, 45, 881.
31. Bartholmai, M.; Schartel, B. Polym Adv Technol 2004, 15, 355.
32. Gilman, J. W.; Kashiwagi, T. Polymer-Clay Nanocomposites; John Wiley & Sons: New York, 2000; p 193.